Supplementary Information

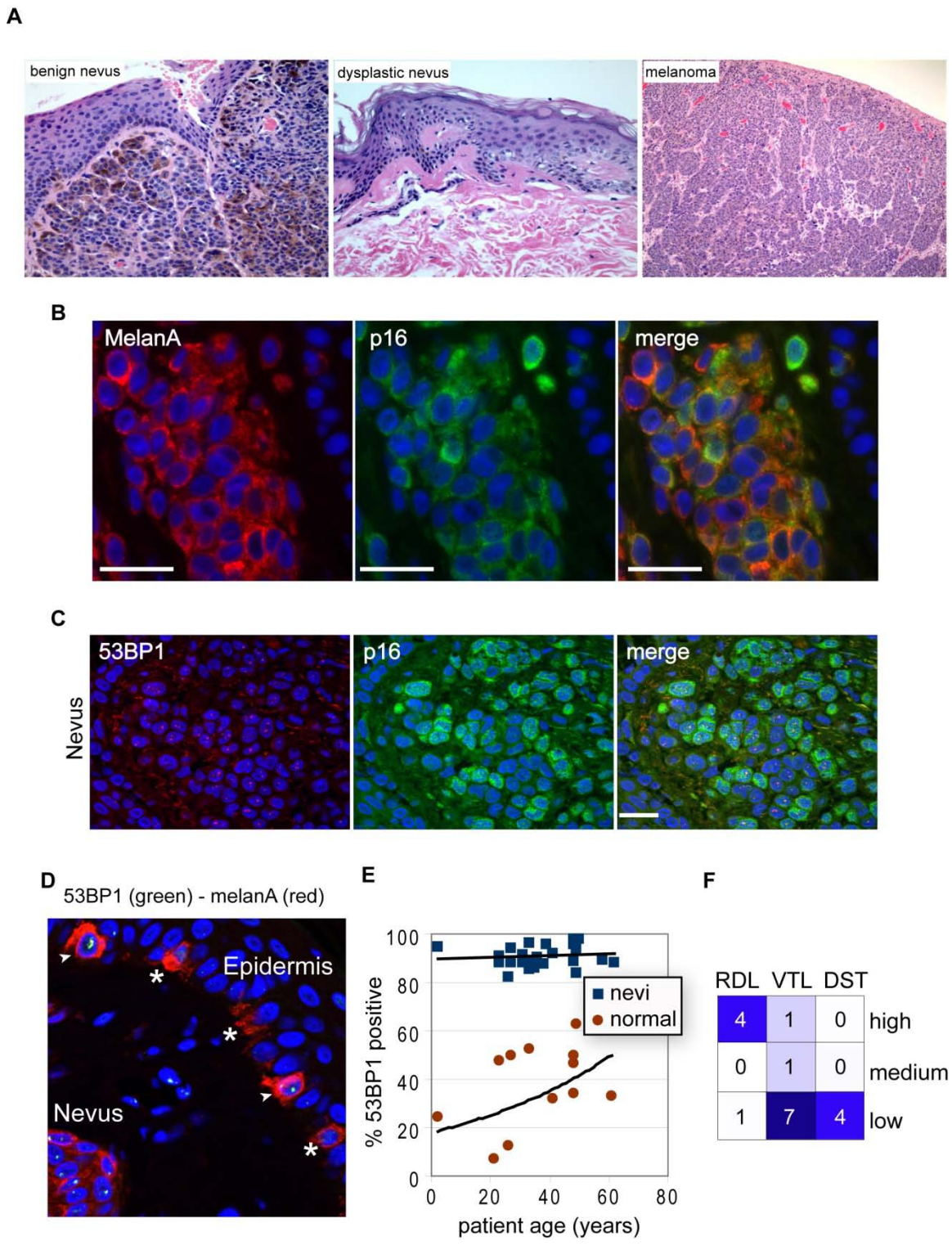

Figure S1. Melanocytic cells of human nevi display DDR foci and a mosaic p16 expression pattern. (**A**) Haematoxylin and eosin (H&E) stained tissue sections from lesions illustrated in Figure 1A. (**B**) Tissue section from a dysplastic nevus was immunostained using antibodies against melanA (red) and p16 (green). DNA was counterstained with DAPI. Scale bar: 25μm. (**C**) Dysplastic nevus was simultaneously immunostained using antibodies against 53BP1 (red) and p16 (green). Note that many cells displaying discrete 53BP1 foci also lack elevated p16 levels. Scale bar: 20μm. (**D**) Human skin tissue section was immunostained using antibodies against melanA (red) and 53BP1 (green). DNA was counterstained with DAPI. *: 53BP1 negative melanocytes; arrow head: 53BP1 positive melanocytes. (**E**) Relationship between patient age and percentage of 53BP1 positive melanocytes in epidermis (normal; brown circles) and in nevi (blue squares). A positive trend between the percent of 53BP1 positive cells and patient age was observed in epidermal melanocytes, although this trend is statistically not significant ($p = 0.182$). No correlation between the percentages of 53BP1 positive melanocytic cells and patient age could be established for nevi ($p = 0.593$). (**F**) Radial growth phase melanoma (RDL), vertical growth phase melanoma (VTL) and melanoma in deep soft tissue (DST) received a score of low (0-20%), medium (21-40%) and high (41-60%) based on the % of cells that stained positive for 53BP1 foci.

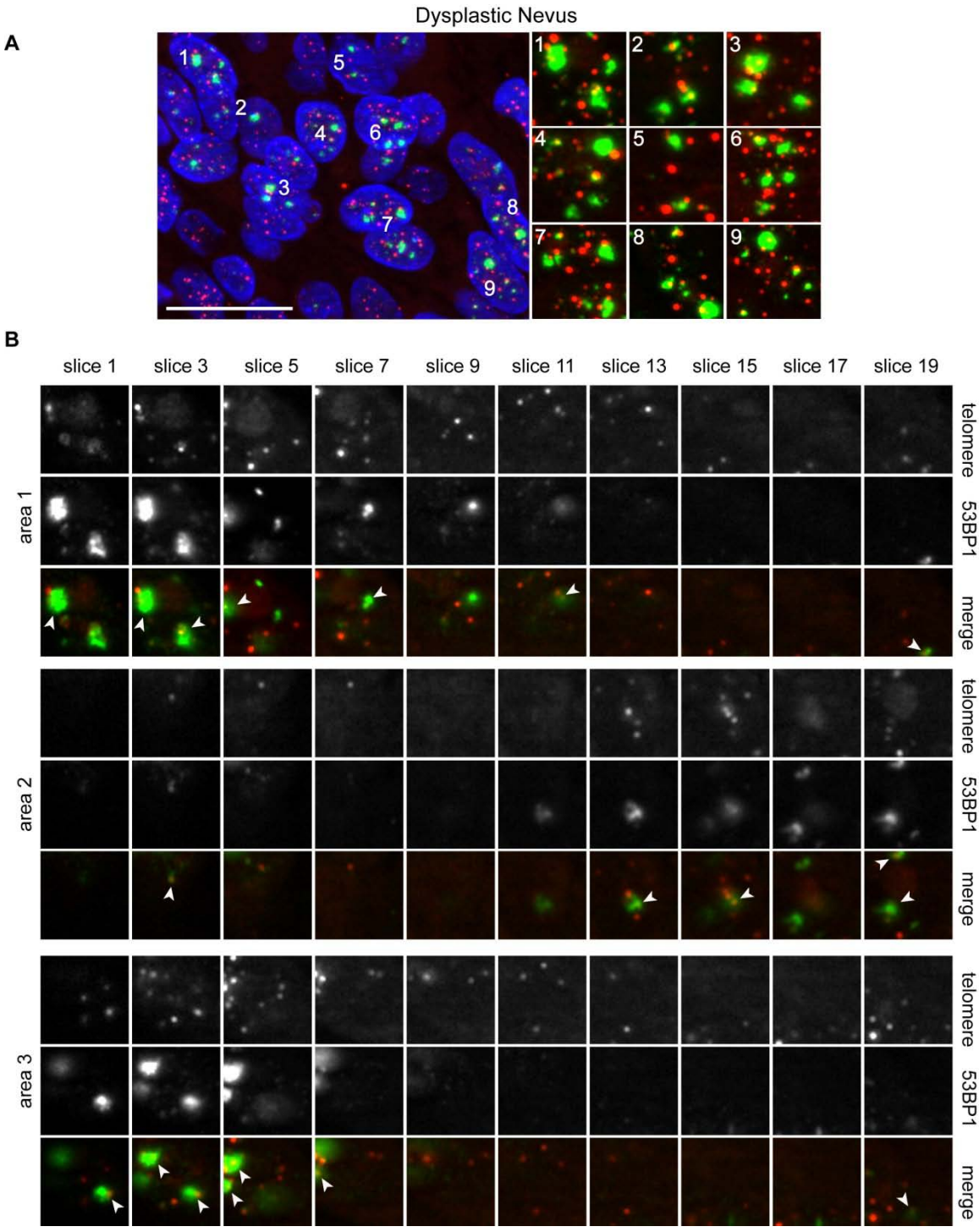
A
Dysplastic Nevus
1
2
3
4
5
6
7
8
9
B
slice 1
slice 3
slice 5
slice 7
slice 9
slice 11
slice 13
slice 15
slice 17
slice 19
area 1
area 2
area 3
telomere
53BP1
merge

continued

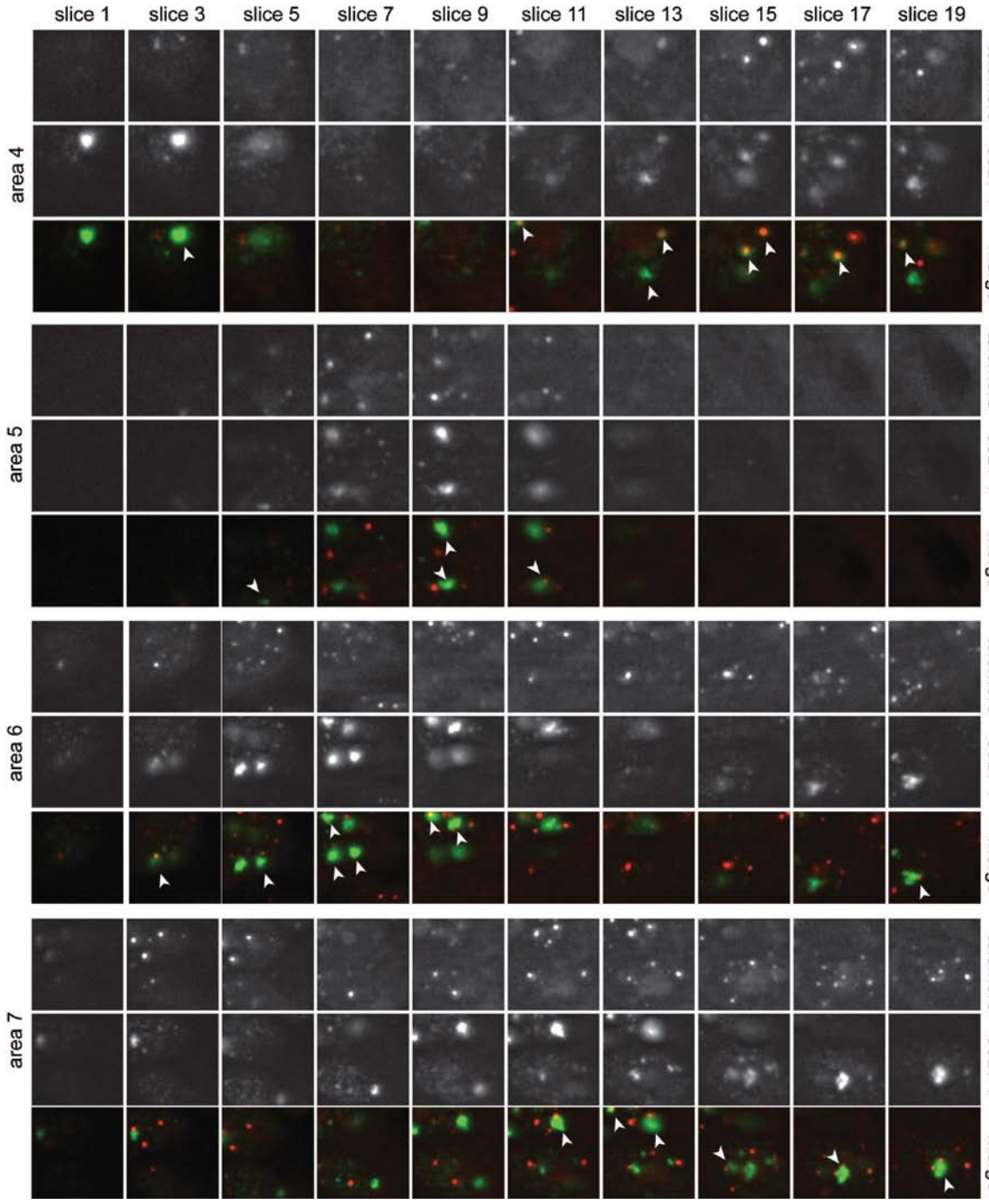
slice 1
slice 3
slice 5
slice 7
slice 9
slice 11
slice 13
slice 15
slice 17
slice 19
area 4
area 5
area 6
area 7
telomere
53BP1
merge

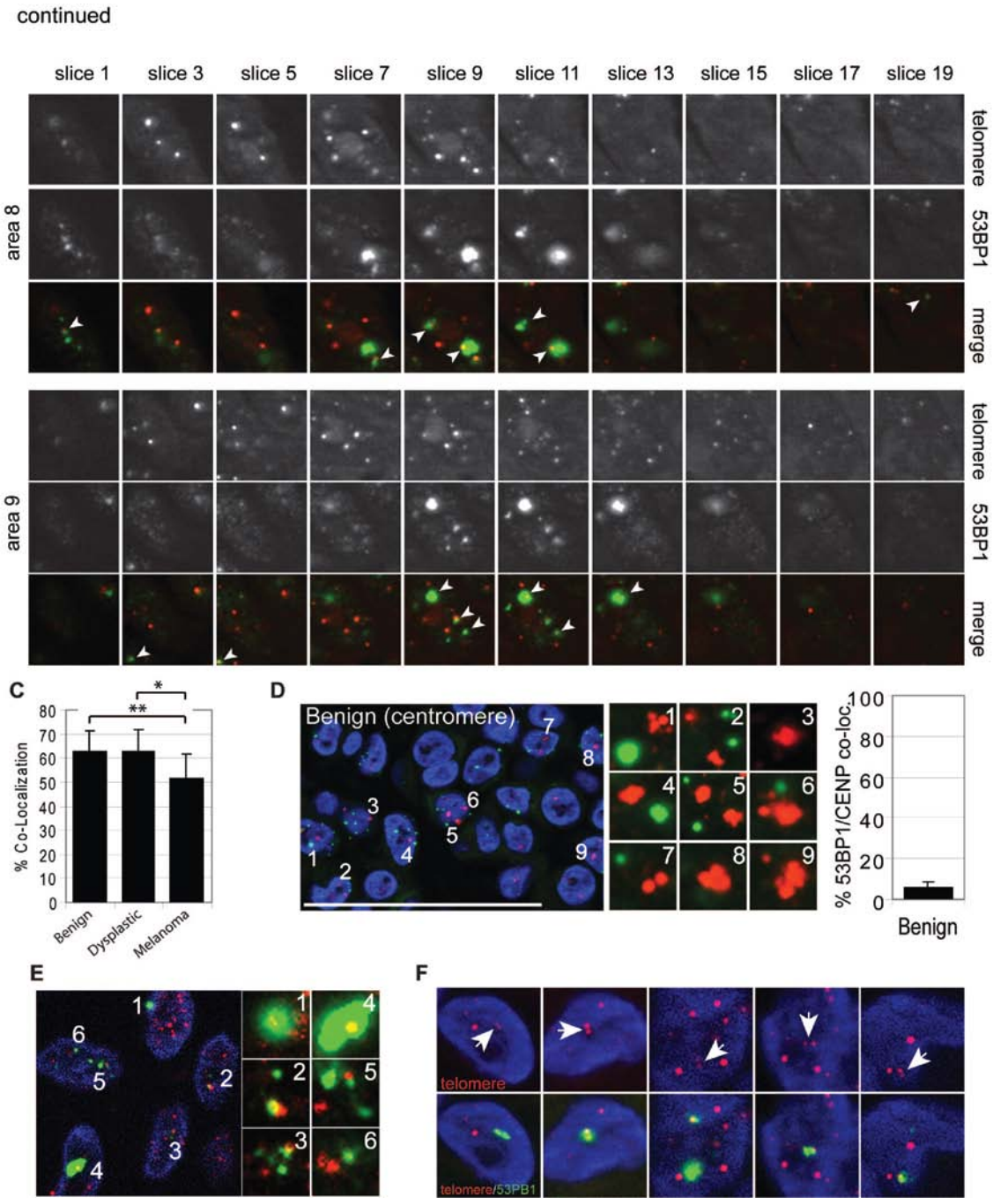

Figure S2. The majority of DDR foci in melanocytic lesions specifically co-localize with telomeres, retain the shelterin component TRF2, and frequently include aberrant telomeric structures. (**A**) 4μm section from a dysplastic nevus was processed by immunoFISH to simultaneously detect 53BP1 (green) and telomeres using a Cy3-labeled telomeric PNA (red). Enlarged versions of the numbered DNA damage foci showing co-

localization with telomeres are shown in the right micrographs. DNA was counterstained with DAPI (blue). Scale bar: 20μm. Image was generated by merging 20 consecutive z-slices using the AxioVision software (Zeiss). Distance between z-slices: 0.3 μm. (**B**) Details of telomere-53BP1 co-localizations for each indicated area in (A). Every second z-slice is shown. Top row: telomere, center row: 53BP1, bottom row: merged image (telomeres: red; 53BP1: green). White arrows indicate 53BP1/telomere co-localizations. (**C**) The mean percentage of 53BP1/telomere co-localization in indicated lesions (± s.d.). Note that only 53BP1 positive melanocytic cells were scored. In melanoma, 53BP1 positive melanocytic cells are primarily observed in radial growth melanoma (see Figure 1c), lesions that have low mitotic figures; * p=0.025; ** p=0.028 by one-way ANOVA followed by Tukey's post hoc test. (**D**) 4μm tissue section from a nevus was simultaneously immunostained using antibodies against the centromeric proteins (green) and 53BP1 (red). Blue: nuclear DNA counterstained with DAPI. Enlarged versions of the numbered DNA damage foci showing lack of co-localization with centromeres are shown in the right micrographs. The % of centromeric foci co-localizing with 53BP1 foci is indicated in the bar graph (± s.d.). A total number of 369 foci from 3 distinct lesions were analyzed. DNA was counterstained with DAPI (blue). Scale bar: 50μm. (**E**) 4μm tissue section from a nevus was simultaneously immunostained using antibodies against TRF2 (red) and 53BP1 (green). Enlarged panels of indicated regions is shown to the right. Note that only a single 0.4 μm z-slice is shown. Scale bar: 10 μm. (**F**) 4μm tissue sections from benign nevi were processed for immunoFISH to detect dysfunctional telomeres. Representative images of individual cells are shown. Red, telomeres visualized using a Cy3-conjugated PNA; green, 53BP1; blue, nuclear DNA counterstained with DAPI. Top

row: arrows point to aberrant telomeric structures such as telomeric doublets that co-localize with 53BP1 foci (bottom row). Only a single 0.4 μm z-slice is shown.

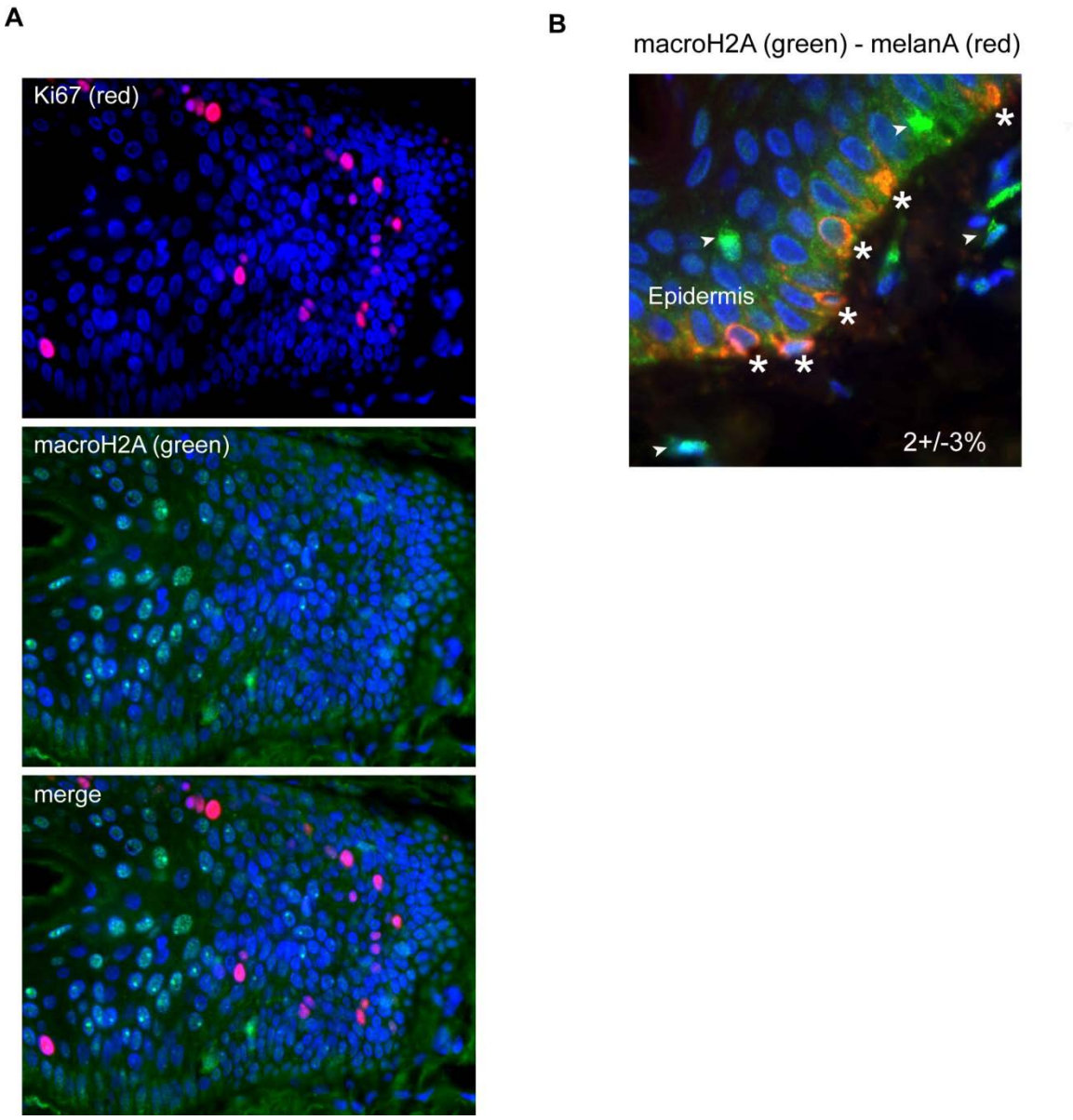

Figure S3. Nuclear macroH2A levels are low in Ki67-positive cells and in normal human epidermal melanocytes. (**A**) Tissue section from a radial growth melanoma was immunostained using antibodies against macroH2A (green) and Ki67 (red). DNA was counterstained with DAPI. (**B**) Dermal tissue section was simultaneously immunostained using antibodies against Melan A (red) and macroH2A (green). DNA was counterstained

with DAPI. *: melanocytes with low levels of macroH2A. Arrows point to macroH2A positive cells. The % of total basal layer melanocytes that displayed elevated macroH2A levels is indicated (± s.d.). A total number of 55 melanocytes from 3 distinct lesions were analyzed.

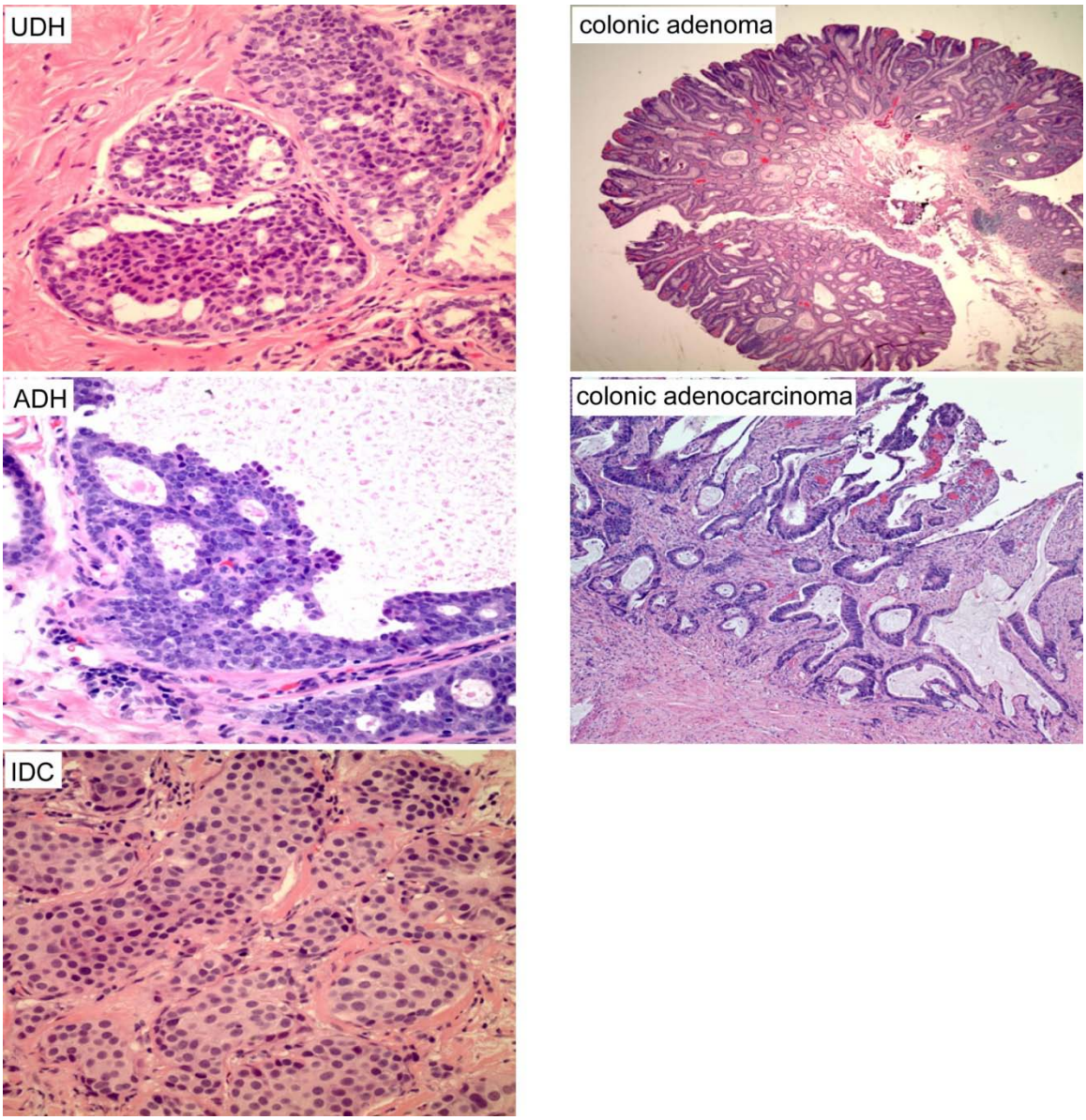

Figure S4. Analyzed tumor tissue. H&E stained tissue sections from lesions illustrated in Figure 2.

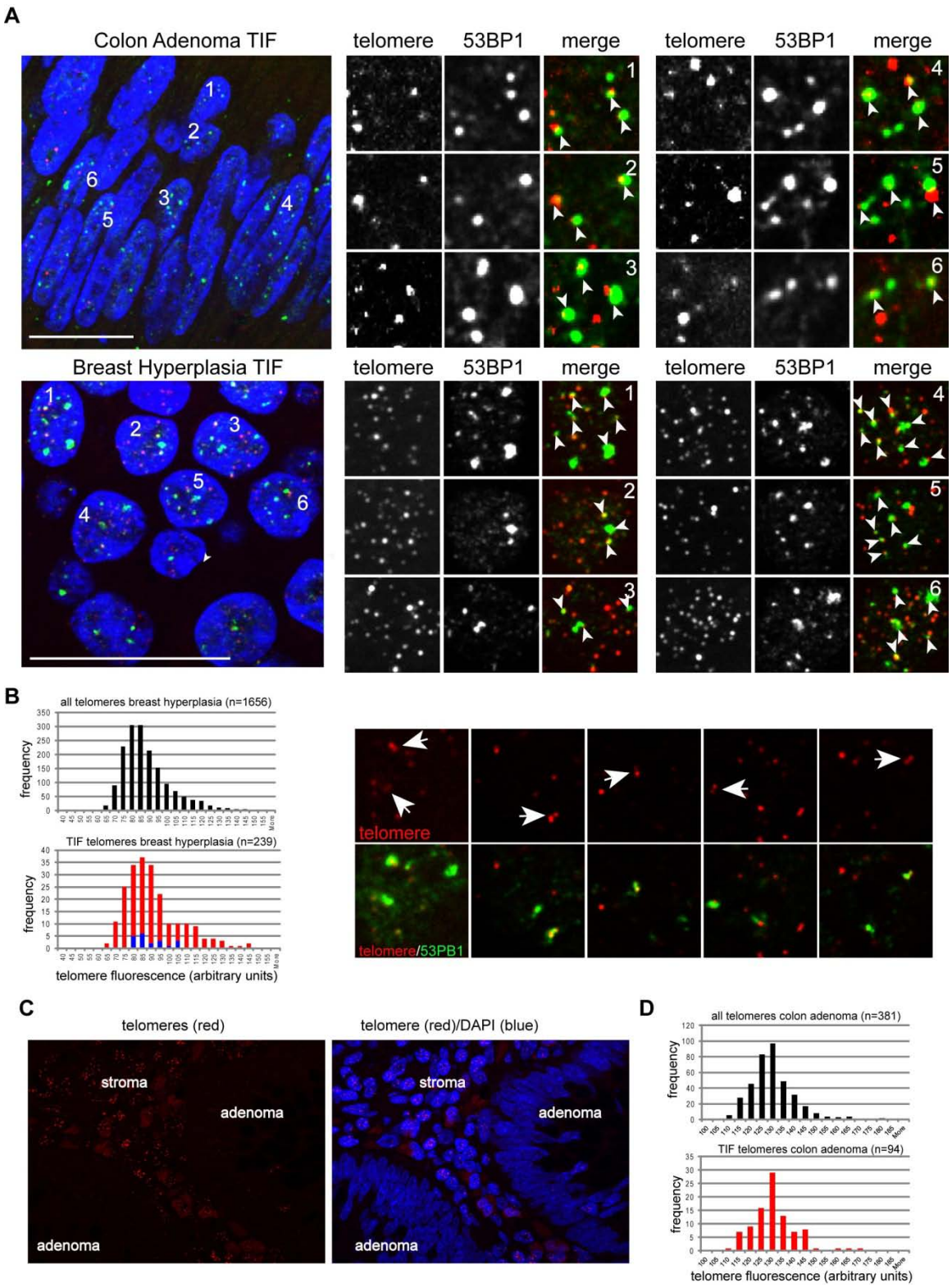

Figure S5. 53BP1 foci in colonic adenomas and ductal hyperplasias of the breast co-localize with telomeric sequences. (**A**) 4μm sections from colon adenoma (top) and

ductal breast hyperplasia (bottom) were processed by immunoFISH to simultaneously detect 53BP1 (green) and telomeres using a Cy3-labeled telomeric PNA (red). Nuclei were counterstained with DAPI (blue). Enlarged versions of the numbered DNA damage foci showing co-localization with telomeres (white arrows) are show to the right. Telomeres (red): left column; 53BP1 (green): center column; merged image: right column. Note that individual z-slices were merged into a single image for illustration purposes. All co-localization studies were performed on individual image stacks as illustrated in supplemental Figure S2. (**B**) Distribution of telomere lengths based on their signal intensities (x-axis; arbitrary units) in cells of ductal hyperplasias of the breast. Top histogram: all telomeric signals analyzed (average signal intensity 86+/-14). Bottom histogram: single (red bars; average signal intensity 88+/-15) and multiple/diffuse (blue bars; average signal intensity 87+/-9) telomeric signals associated with 53BP1 foci. n: number of telomeric signals analyzed. Micrographs: 4μm tissue sections from ductal hyperplasias of the breast were processed for immunoFISH to detect dysfunctional telomeres. Representative images of individual cells are shown. Red, telomeres visualized using a Cy3-conjugated PNA; green, 53BP1; blue, nuclear DNA counterstained with DAPI. Top row: arrows point to aberrant telomeric structures such as telomeric doublets that co-localize with 53BP1 foci (bottom row). Only a single 0.4 μm z-slice is shown. (**C**) Telomeres of a colonic adenoma were stained with a Cy3 labeled-peptide nucleic acid complementary to telomeric repeats (red). DNA was counterstaind with DAPI (blue). Stroma and adenoma are indicated. (**D**) Distribution of telomere lengths based on their signal intensities (x-axis; arbitrary units) in cells of tubular adenomas. Top histogram: all telomeric signals analyzed (average signal intensity 128+/-

12). Bottom histogram: single (red bars; average signal intensity 129+/-10). n: number of telomeric signals analyzed

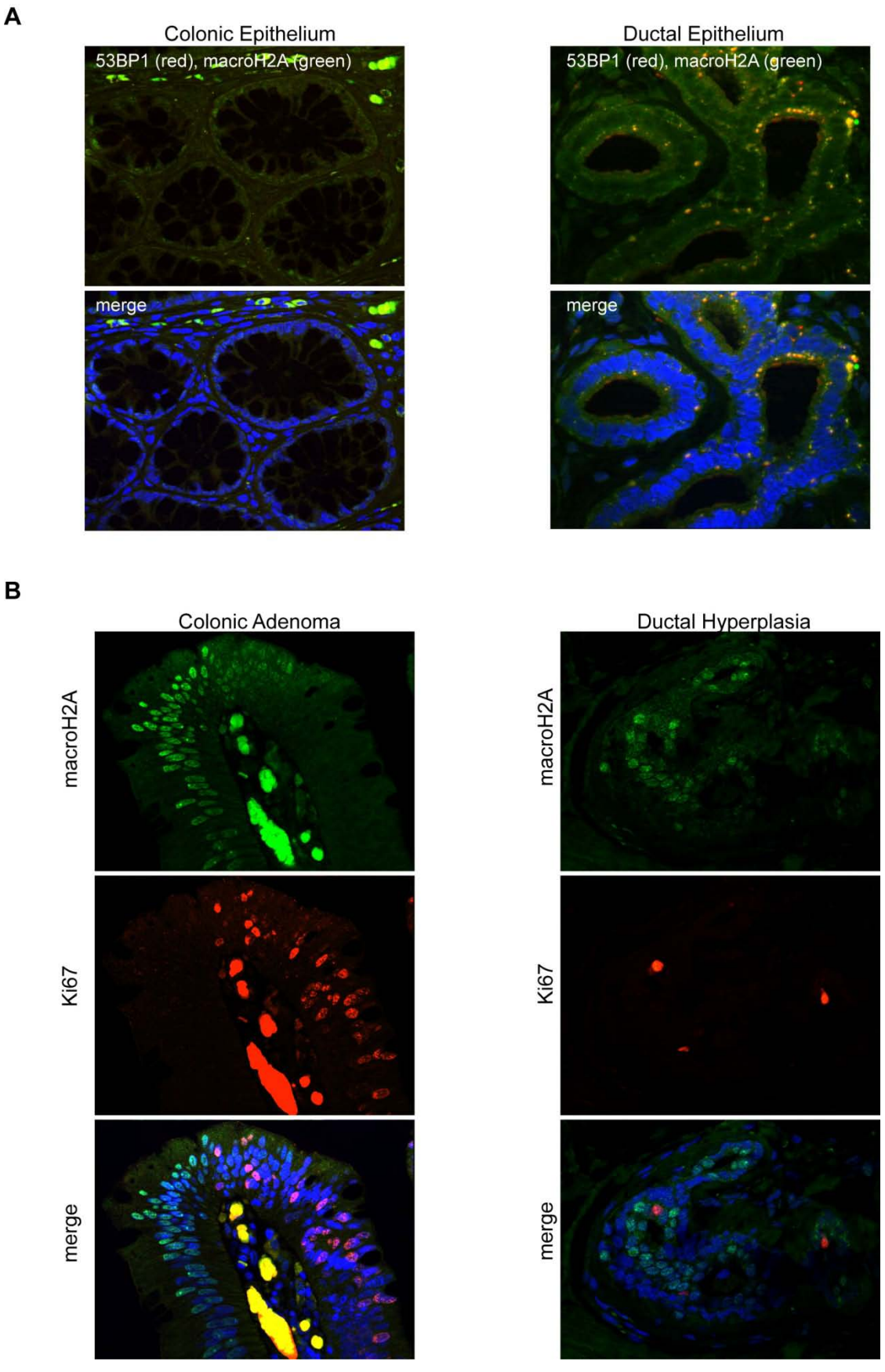
A
Colonic Epithelium
53BP1 (red), macroH2A (green)
merge
Ductal Epithelium
53BP1 (red), macroH2A (green)
merge
B
Colonic Adenoma
Ductal Hyperplasia
macroH2A
Ki67
merge
macroH2A
Ki67
merge

Figure S6. Nuclear macroH2A levels are undetectable in normal epithelium of breast and colon and in Ki67-positive epithelial cells of colonic adenomas and ductal hyperplasias of the breast. (**A**) Normal colonic- (left column) and ductal- (right column) epithelium adjacent to hyperplastic regions was immunostained using antibodies against 53BP1 (red) and macroH2A (green). DAPI: blue. (**B**) Tissue section from indicated cancer precursor lesions were immunostained using antibodies against macroH2A (green) and Ki67 (red). DNA was counterstained with DAPI. Note that the bright yellow stain in the center of the image is due to high auto-fluorescence in the tissue.

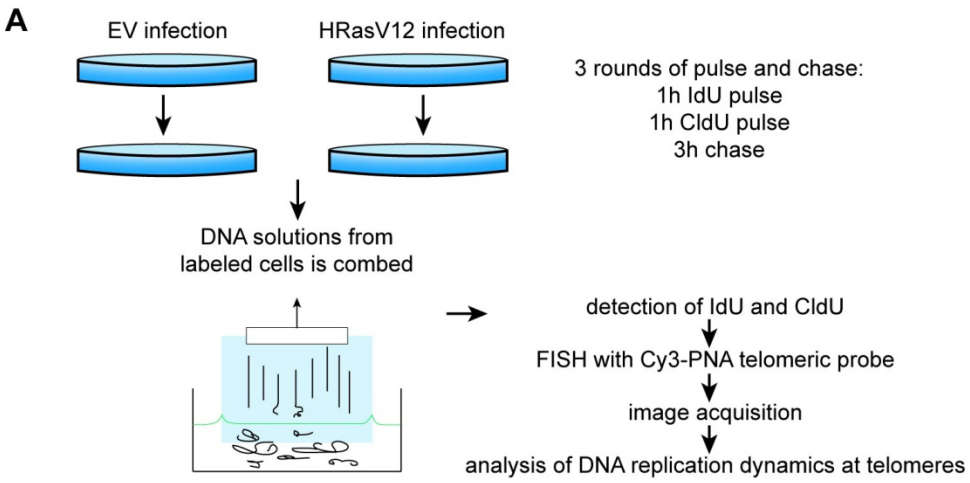
A
EV infection
HRasV12 infection
3 rounds of pulse and chase:
1h IdU pulse
1h CldU pulse
3h chase
DNA solutions from
labeled cells is combed
detection of IdU and CldU
FISH with Cy3-PNA telomeric probe
image acquisition
analysis of DNA replication dynamics at telomeres

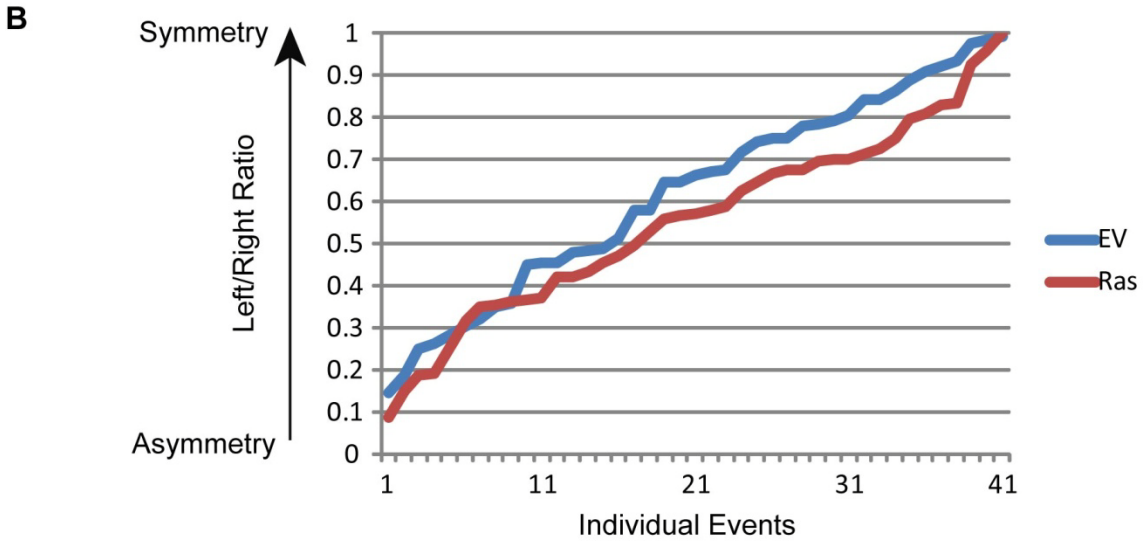
B
Symmetry
Asymmetry
Left/Right Ratio
1
0.9
0.8
0.7
0.6
0.5
0.4
0.3
0.2
0.1
0
1
11
21
31
41
Individual Events
EV
Ras

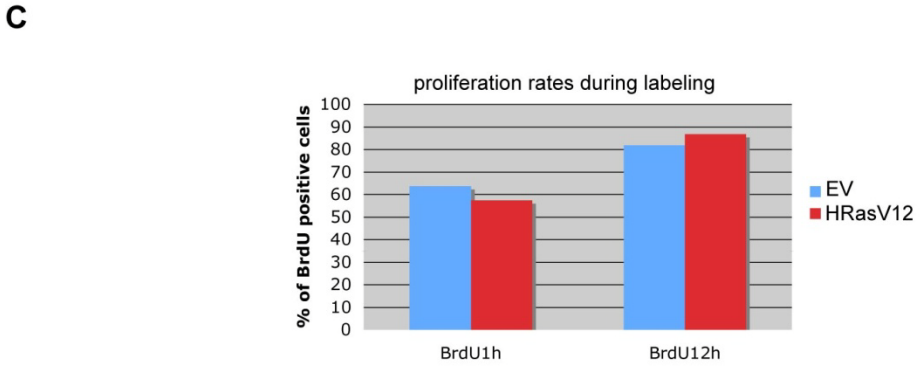
C
proliferation rates during labeling
% of BrdU positive cells
100
90
80
70
60
50
40
30
20
10
0
BrdU1h
BrdU12h
EV
HRasV12

Figure S7. Telomeric DNA combing. (**A**) Schematic illustrating experimental design. (**B**) Whole genome analysis of fork stalling was performed by assessing the symmetry of DNA replication fork progression and by generating a ratio between left and right fork speed derived from the same DNA replication origin. A ratio of 0 indicates a completely asymmetric fork; as the ratio increases, the level of asymmetry decreases; a ratio of 1 indicates completely symmetric DNA replication fork progression. All the ratios (n=41) were sorted from the lowest to the highest values and plotted in this graph. Telomeric loci were excluded from this analysis. EV, control cells; Ras, H-RasV12 expressing cells. (Wilcoxon test, $p <= 0.9963$). (**C**) Percentage of control- (EV) and HRasV12 -transduced mouse cells that stained positive for BrdU. BrdU was added to the culture medium for indicated times.

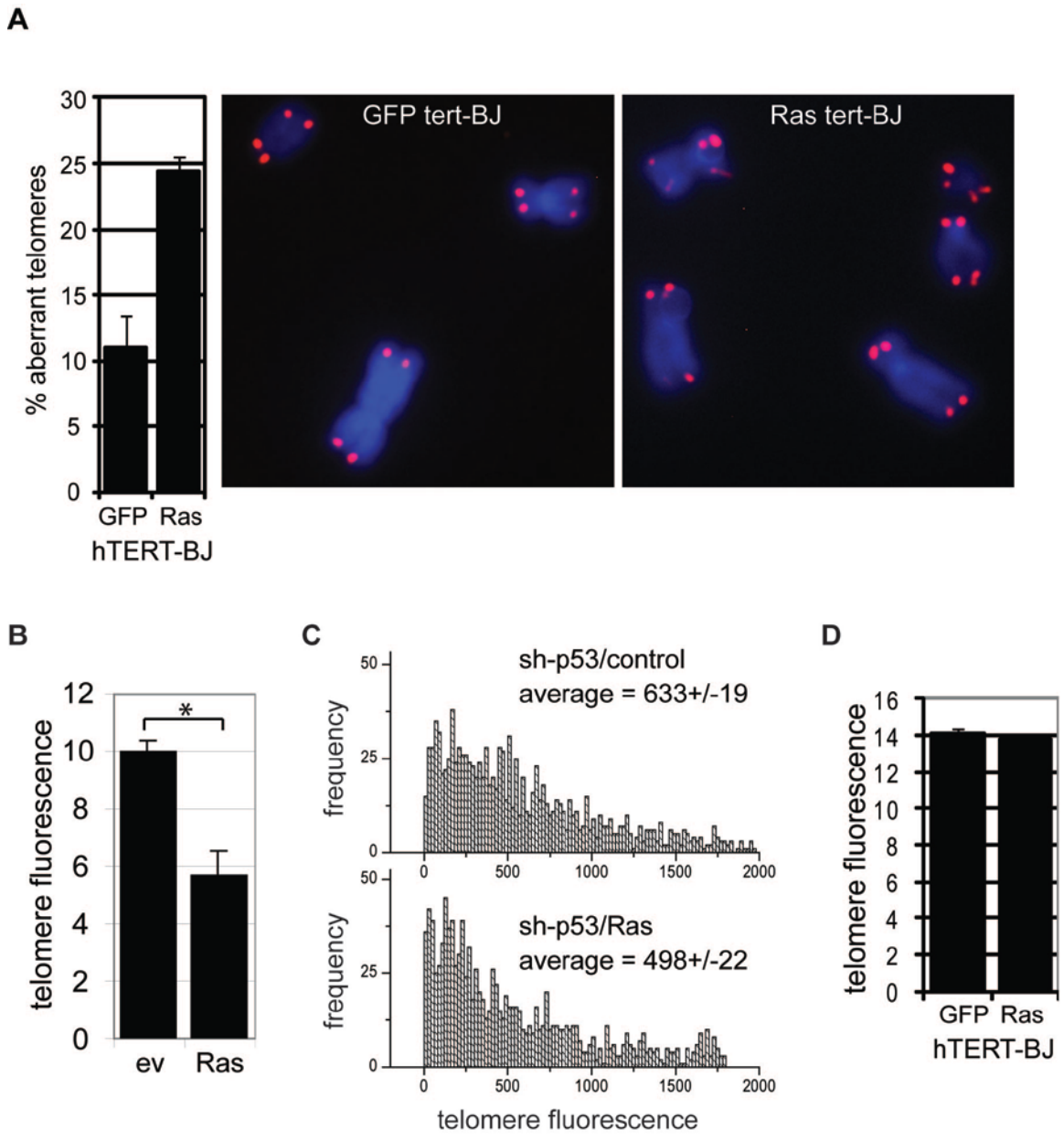

Figure S8. Oncogenic Ras expression induces fragile telomeres in hTERT expressing cells and telomere shortening in normal and p53 knockdown cells that lack hTERT expression.

(**A**) Metaphases from hTERT expressing BJ cells that were contact inhibited, transduced with lentivirus encoding GFP (as a control) and H-RasV12, and subsequently released into colcemid containing medium. Bar graph: percentage of aberrant telomeric structures

(± s.d.) in GFP (12 metaphases) and Ras (19 metaphases) expressing cells (n=2). Quantitation of aberrant telomere structures was performed as in Figure 4A. Mircrographs: representative images of metaphase telomeres in indicated cells. Chromosome ends were labeled using a telomeric Cy3 conjugated-PNA (red). Metaphase chromosomes were counterstained with DAPI (blue). (**B**) BJ cells were transduced with retrovirus encoding H-RasV12 (Ras) or empty vector (ev). Telomere lengths were measured by flow-FISH after Ras expressing cells entered senescence (21 days following retroviral transduction). *: $p<0.001$ by unpaired t-test. (**C**) Distribution of the telomere lengths of proliferating BJ fibroblasts in which p53 had been knocked down using shRNA. Telomere lengths were measured by q-FISH. The average telomere fluorescence signal is indicated (± s.d.). Top: p53 knockdown cells transduced with empty vector expressing retrovirus; bottom: p53 knockdown cells transduced with H-RasV12 expressing retrovirus. (**D**) Contact inhibited hTERT expressing BJ cells were transduced with lentivirus encoding GFP (control) or Ras followed by release into colcemid-containing medium. These cells therefore proceeded through only one S phase, similar to the data shown in Figure 4B. Telomere lengths were measured by flow-FISH (y-axis arbitrary units, mean ± s.d.).

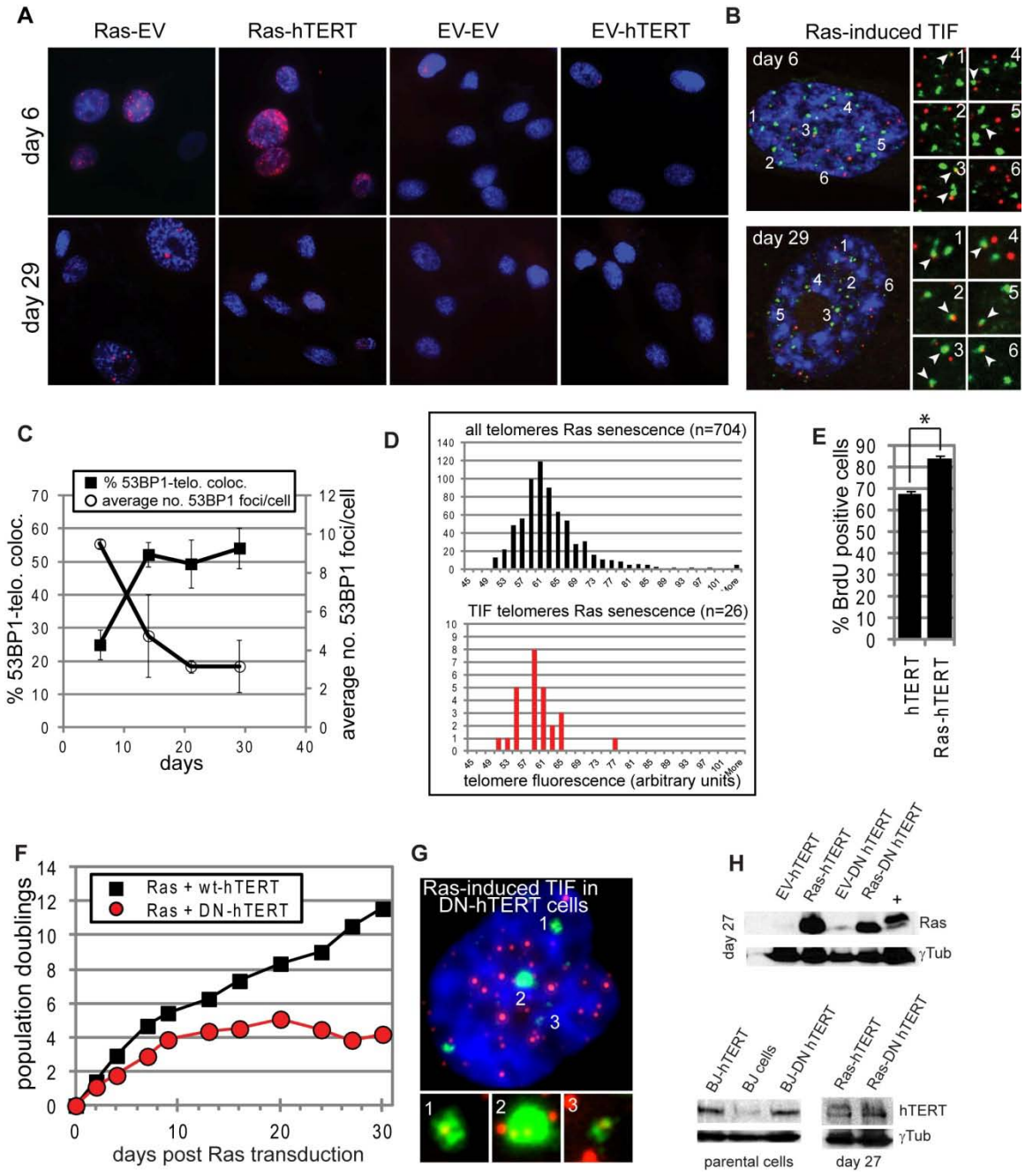

Figure S9. Oncogenic Ras expression induces transient non-telomeric and persistent telomeric DDR foci in the absence of catalytically active hTERT.

(**A**) 53BP1 (red) immunostaining at day 6 (top row) and 29 (bottom row) following transduction with indicated combinations of retroviruses. Nuclear DNA was counterstained with DAPI (blue). (**B**) Micrographs: dysfunctional telomeres in Ras

expressing cells at days 6 (top) and 29 (bottom) following retroviral transduction. TIF were visualized by telomere immunoFISH to simultaneously detect 53BP1 (green) and telomeres using a Cy3-labeled telomeric PNA (red). Enlarged versions of the numbered areas are showing to the right. White arrows indicate 53BP1-telomere co-localizations. (**C**) The percentages of 53BP1 foci co-localizing with telomeres in DDR positive cells (left y-axis; solid squares) vs. the average number of 53BP1 foci per cell in DDR positive cells (right y-axis; open circles). (**D**) Distribution of telomere lengths based on their signal intensities (x-axis; arbitrary units) in Ras expressing cells 29 days after retroviral transduction. Top histogram: all telomeric signals analyzed (average signal intensity 63+/-9). Bottom histogram: single (red bars; average signal intensity 59+/-50). n: number of telomeric signals analyzed. (**E**) percentage of BrdU positive cells in Ras-hTERT (day 29) and parental hTERT expressing BJ cells demonstrating higher proliferation rates in ras expressing cells. BrdU was added for 8 hours. * p=0.0002 (**F**) Growth curve of wt-hTERT (black squares) and a catalytically inactive dominant negative mutant of hTERT (DN-hTERT; red circles) expressing BJ cells transduced with H-RasV12. (**G**) Dysfunctional telomeres in Ras/DN-hTERT expressing BJ cells 27 days following Ras transduction. Red, telomeres; green, γH2AX; blue, nuclear DNA counterstained with DAPI. Enlarged and numbered regions of TIF are shown below. (**H**) Immunoblots demonstrating Ras (top) and hTERT (bottom) expression levels in indicated cells 27 days following Ras transduction. Parental cells: cells used for Ras transduction. +: positive control showing high Ras expression levels in a separate proliferating Ras/hTERT expressing cell line. Bottom immunoblots demonstrate similar expression levels of wt-

hTERT and DN-hTERT in parental cells used for Ras transduction and in Ras expressing cells 27 days following Ras transduction. γTubulin served as loading control.

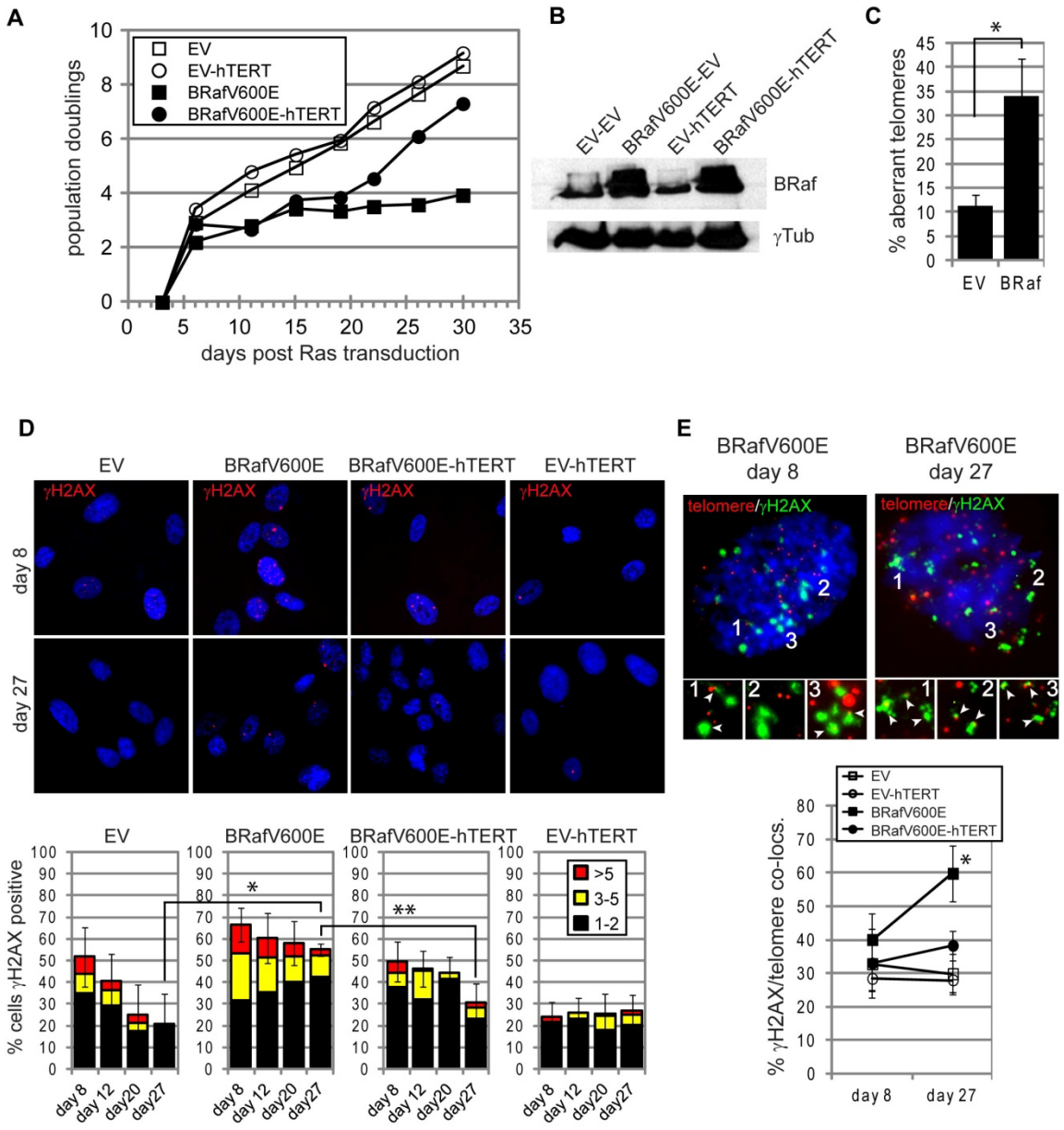

Figure S10. Oncogenic BRafV600E causes cellular senescence that is stabilized by telomere dysfunction in human cells. (**A**) Growth curves of BJ cells and hTERT expressing BJ cells transduced with oncogenic BRafV600E. (**B**) Immunoblot demonstrating high BRaf expression levels 28 days after retroviral transduction. γTubulin served as loading control. EV: empty vector. (**C**) Percentage (±s.d.) of aberrant telomeric structures defined as diffuse telomeric signals, multi-telomeric signals, different signal

intensities at sister telomeres detected on metaphase chromosomes in control (EV) and BRafV600E (BRaf) expressing BJ cells 48h after retroviral transduction. *p=0.0076 (**D**) γH2AX (red) immunostaining at day 6 (top row) and 27 (bottom row) following transduction with indicated retroviruses. Nuclear DNA was counterstained with DAPI (blue). Bar graphs illustrate quantitations of γH2AX positive cells that displayed either 1-2 (black bars), 3-5 (yellow bars) or more that 5 (red bars) γH2AX foci per cell nucleus. A minimum of 111 cells were scored per group and time point. *p=0.0021; ** p=0.0009 by unpaired t test (**E**) Dysfunctional telomeres in Ras expressing cells at indicated days following BRafV600E transduction. TIF were visualized by telomere immunoFISH to simultaneously detect γH2AX (green) and telomeres using a Cy3-labeled telomeric PNA (red). Enlarged versions of the numbered areas are showing to the bottom. White arrows indicate γH2AX -telomere co-localizations. Line graph illustrates quantitation of γH2AX -telomere co-localizations in γH2AX positive cells at indicated days following retroviral transductions. An average of 62 cells were scored per group and time point. *p<0.002.

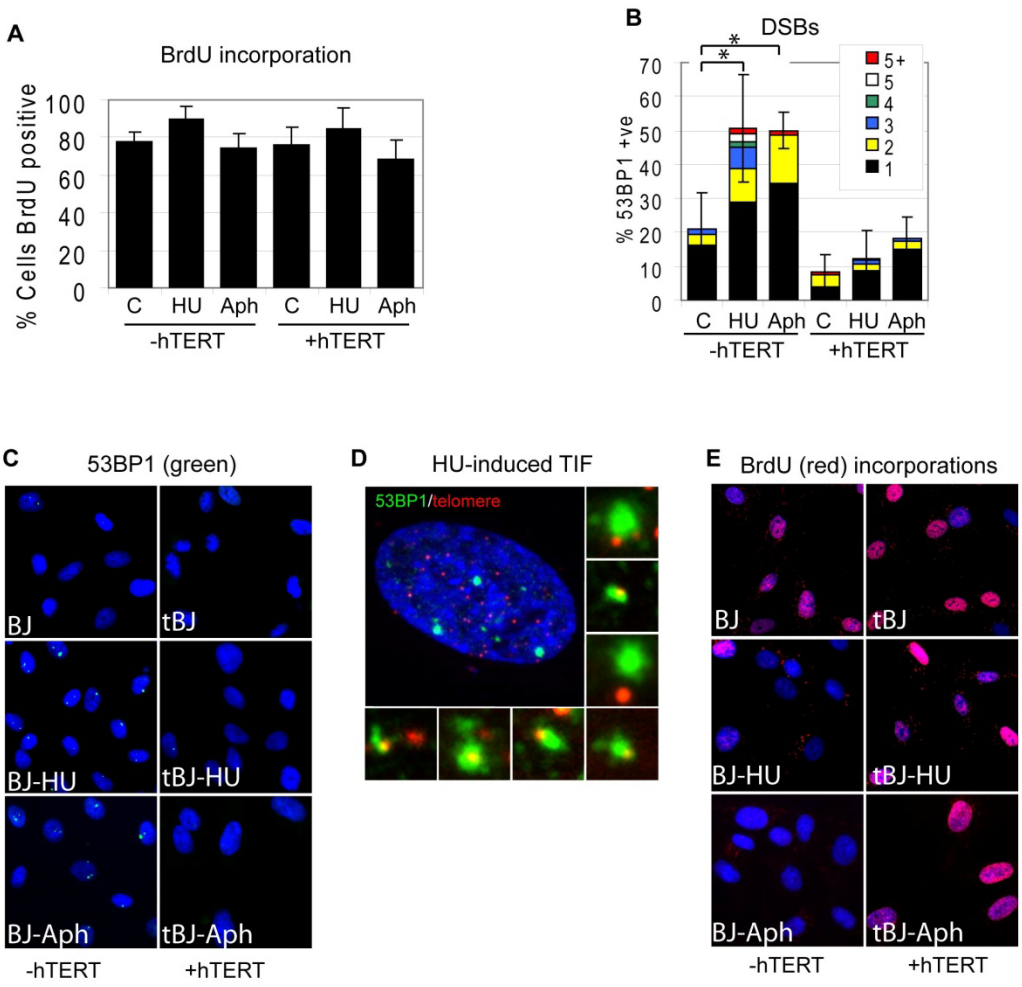

Figure S11. Chronic exposure to hydroxyurea and aphidicolin causes TDIS in normal human fibroblasts. BJ cells (-hTERT) and hTERT-expressing BJ cells (+hTERT) were incubated with low concentrations of hydroxyurea (HU; 50 μM) and aphidicolin (Aph; 0.3μM) for 4 days in the presence of BrdU. (**A**) % ofBrdU positive cells. BrdU was added at the time of drug exposure. Cells were analyzed 48h following addition of BrdU/drug. (**B**) % of 53BP1 positive cells following the 4 days of drug incubations. The frequency of DNA damage foci per cell nucleus is indicated by colored bars (± s.d.); * p=0.003 by paired t-test. Representative images of 53BP1 foci (**C**), TIF (**D**) and BrdU incorporations (**E**). tBJ: hTERT expressing BJ cells.

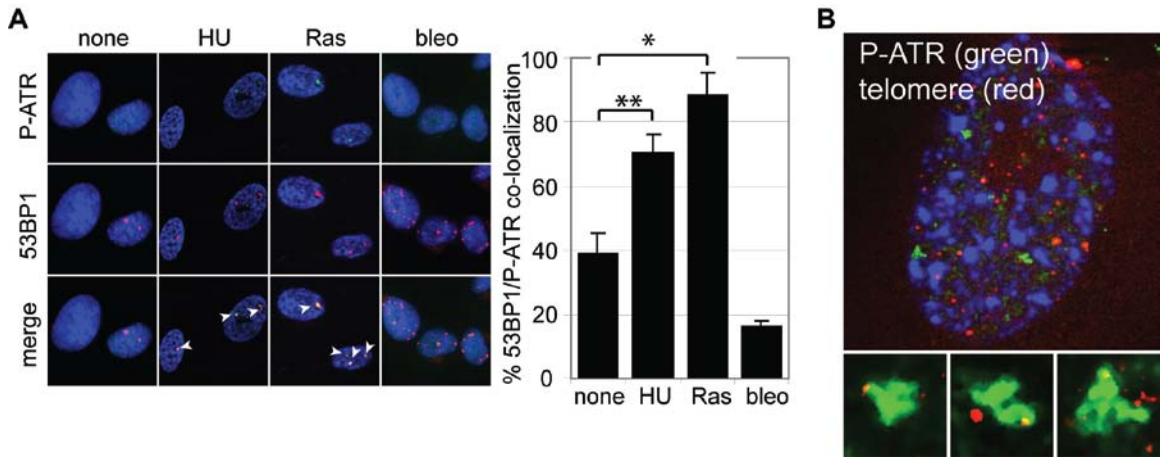

Figure S12. ATR phosphorylated at residue Ser428 co-localizes with 53BP1 and telomeres only in cells exposed to DNA replication stress. (**A**) BJ cells were immunostained with antibodies against phospho-ATR(Ser428; green) and 53BP1(red). DNA replication stress was cause by incubating BJ cells with hydroxyurea (HU, 50μg/ml, 4 days), and H-RasV12 (Ras). As a control, bleomycin treated (bleo, 4μg/ml, 4h) and untreated BJ cells (none) were also immunostained. The % of 53BP1 foci co-localizing with P-ATR is indicated in the bar graph (± s.d.); *p<0.001; **p=0.004 by one-way ANOVA followed by Tukey's posthoc test. (**B**) Senescent H-RasV12 transduced BJ cells were processed by immunoFISH to simultaneously detect phosphor-ATR(Ser428; green; P-ATR) and telomeres (red). Bottom micrographs: enlarged ATR(Ser428; P-ATR) foci showing co-localization with telomeres.